Porous Metals with Developing Anisotropy: Constitutive Models, Computational Issues and Applications to Deformation Processing

M. Kailasam[1], **N. Aravas**[2], **P. Ponte Castañeda**[3]

Abstract: A constitutive model for a porous metal subjected to general three-dimensional finite deformations is presented. The model takes into account the evolution of porosity and the development of anisotropy due to changes in the shape and the orientation of the voids during deformation. A methodology for the numerical integration of the elastoplastic constitutive model is developed. Finally, some sample applications to plane strain extrusion and compaction of a porous disk are considered using the finite element method.

1 Introduction

Building on earlier work Ponte Castañeda and Zaidman (1994, 1996); Kailasam, Ponte Castañeda and Willis (1997a), Kailasam and Ponte Castañeda (1997, 1998) proposed a general constitutive theory to model effective behavior and microstructure evolution in composites and porous materials undergoing finite deformations. The theory is based on a rigorous homogenization analysis and is applicable to heterogeneous materials with "particulate" microstructures, consisting of random distributions of families of inclusions (or voids) of various shapes and orientations embedded in a matrix.

In this work, the special case of porous metals is considered in detail. Initially, the pores are assumed to be aligned ellipsoids of given shape (in particular, spherical) that are distributed randomly in a perfectly plastic matrix (metal). Under finite plastic deformation, the voids are assumed to remain aligned ellipsoids, but to change their volume, shape and orientation. At every point in the homogenized continuum, a "representative" ellipsoid is considered with principal axes defined by the unit vectors $\mathbf{n}^{(1)}, \mathbf{n}^{(2)}, \mathbf{n}^{(3)} = \mathbf{n}^{(1)} \times \mathbf{n}^{(2)}$ and corresponding principal lengths a, b, and c. The homogenized continuum is locally orthotropic, with the local axes of orthotropy coinciding with the principal axes of the representative ellipsoid. The basic "internal variables" characterizing the state of the microstructure at every point in the homogenized continuum are given by the local void volume fraction or porosity (f), the two aspect ratios of the local representative ellipsoid ($w_1 = c/a$ and $w_2 = c/b$) and the orientation of the principal axes of the ellipsoid ($\mathbf{n}^{(1)}, \mathbf{n}^{(2)}, \mathbf{n}^{(3)}$). Although hardening of the plastic matrix could easily be incorporated [see, for example, Aravas (1992)], in this work the matrix phase is taken to be perfectly plastic, so as to isolate the hardening or softening effects generated by the evolution of the microstructure. The model of Kailasam and Ponte Castañeda (1997, 1998) originally assumed that the matrix was nonlinearly viscous, including *rigid*-perfectly plastic behavior in the rate-insensitive limit. Unfortunately, the homogenization analysis of materials made up of *elastic*-perfectly plastic constituents is not straightforward. The difficulty arises, in part, due to the fact that the macroscopic elastic and plastic strains are *not*, in general, the averages of their microscopic counterparts Suquet (1985). In addition, memory effects can become significant. Thus, it is not entirely possible to eliminate all the microscopic field variables in the homogenization analysis. In particular, the macroscopic constitutive laws for such materials require the knowledge of the plastic strains at every point in the material, and therefore of an infinite number of internal variables. Fortunately, as pointed by Suquet (1985), a simplified approach is possible when the elastic strains are small.

For the case of interest here (porous metals), the voids do not store any energy and, therefore, elastic effects can arise only from the elasticity of the matrix phase. Also, for metals, the plastic deformations can be assumed to be large compared to the elastic deformations. These hypotheses suggest the use of an approximate approach, where (i) the elastic and plastic response of the materials are treated separately, and later combined to generate the complete elastic-plastic response; and (ii) the evolution of the microstructure in the material undergoing finite deformation is taken to be controlled solely by the plastic deformations. The development of such a theory for elastic-plastic porous materials requires that the constitutive theory proposed by Kailasam and Ponte Castañeda (1997, 1998) for rigid-plastic materials be extended in an appropriate manner. Therefore, constitutive laws are first derived to characterize the instantaneous constitutive behavior of the porous material in the elastic regime and then corresponding laws are generated for the plastic regime. The final step in the development of the constitutive theory is to obtain evolution equations for the various microstructural variables.

For convenience, the resulting constitutive model is henceforth referred to as the *anisotropic* model, to distinguish it from more standard *isotropic* models, such as the model of Gurson

[1] Hibbitt, Karlsson and Sorensen, Inc., 1080 Main St., Pawtucket, RI 02860, USA

[2] Department of Mechanical and Industrial Engineering, University of Thessaly, 38334 Volos, Greece

[3] Department of Mechanical Engineering and Applied Mechanics, University of Pennsylvania, Philadelphia, PA 19104-6315, USA

(1977), in which the voids are assumed to remain spherical as the porous metal deforms.

The numerical implementation of the developed anisotropic elastic-plastic model in a finite element program and an algorithm for the numerical integration of the elastoplastic equations are also presented. Finally, use is made of the anisotropic constitutive theory in the context of the developed finite element formulation to model several forming processes including plane-strain extrusion of porous metals Govindarajan (1992) and compaction of a tapered disk made of porous metal Zavaliangos and Anand (1993); Parteder, Riedel and Kopp (1999). Comparisons are made between the predictions of the anisotropic model and those of the isotropic Gurson model. The most significant difference between the anisotropic and Gurson models is, of course, that while the anisotropic model incorporates the effects of the evolving anisotropy in the porous material as it undergoes deformation, the Gurson model takes the material to remain isotropic throughout the deformation process. In addition, it is found that the evolving anisotropy in the porous material can significantly affect its macroscopic response.

Standard notation is used throughout. Boldface symbols denote tensors, the orders of which are indicated by the context. All tensor components are written with respect to a Cartesian coordinate system, and the summation convention is used for repeated Latin indices, unless otherwise indicated. A superscript T indicates the transpose of a second-order tensor and a superposed dot the material time derivative. Let $\mathbf{a}$ and $\mathbf{b}$ be vectors, $\mathbf{A}$ and $\mathbf{B}$ second-order tensors, and $\mathbf{C}$ and $\mathbf{D}$ fourth-order tensors; the following products are used in the text $(\mathbf{a}\otimes\mathbf{b})_{ij}=a_ib_j$, $(\mathbf{Aa})_i=A_{ij}a_j$, $(\mathbf{AB})_{ij}=A_{ik}B_{kj}$, $\mathbf{A}\cdot\mathbf{B}=A_{ij}B_{ij}$, $(\mathbf{A}\otimes\mathbf{B})_{ijkl}=A_{ij}B_{kl}$, $(\mathbf{CA})_{ij}=C_{ijkl}A_{kl}$, $(\mathbf{AC})_{ij}=A_{kl}C_{klij}$, and $(\mathbf{CD})_{ijkl}=C_{ijmn}D_{mnkl}$. The inverse of a symmetric fourth-order tensor ($C_{ijkl}=C_{klij}$) is defined so that $\mathbf{CC^{-1}}=\mathbf{I}$, where $\mathbf{I}$ is the symmetric fourth-order identity tensor with Cartesian components $I_{ijkl}=(\delta_{ik}\delta_{jl}+\delta_{il}\delta_{jk})/2$.

2 Description of the Constitutive Model

In this section, the *anisotropic* constitutive model for porous metals is described. The main ingredient in the derivation of the constitutive relations is the variational procedure of Ponte Castañeda (1991) which is used to estimate the effective properties of the nonlinear porous material in terms of an appropriate "linear comparison composite." In turn, the properties of the relevant linear comparison composite are obtained from Hashin-Shtrikman estimates of Ponte Castañeda and Willis (1995) for composites with "particulate" microstructures. In the original derivation, the elastic strains, being small, were neglected and ideal plasticity was considered as the appropriate limit of a nonlinearly viscous solid. Here, mostly for numerical convenience, elastic effects are incorporated. As discussed in the Introduction, an approximate approach is used, where the elastic and plastic response of the porous materials are treated independently, and later combined to obtain the full elastic-plastic response. Thus, the average rate-of-deformation tensor $\bar{\mathbf{D}}$ at every point in the porous material is taken to be of the form

$$\bar{\mathbf{D}}=\bar{\mathbf{D}}^e+\bar{\mathbf{D}}^p, \tag{1}$$

where $\bar{\mathbf{D}}^e$ and $\bar{\mathbf{D}}^p$ are the elastic and plastic parts.

For simplicity and because spatial distributions effects are not expected to be significant for porous materials [see Kailasam, Ponte Castañeda and Willis (1997b)], the assumption is made, within the context the estimates of Ponte Castañeda and Willis (1995), that the "shape" and "orientation" of the two-point correlation function characterizing the distribution of the voids in space has the same shape and orientation as the voids themselves. Then, it can be assumed that, as the material deforms, both the voids and their distribution evolve with identical shapes and orientations. This allows the use of the simplified linear-elastic estimates of Willis (1977, 1978), as was done by Ponte Castañeda and Zaidman (1994) in their original treatment of microstructure evolution in porous metals. In particular, this means that the porous material develops and maintains general orthotropic symmetry, with axes aligned with the axes of the ellipsoidal voids.

The model is presented next in three parts. The first part of the model deals with the elastic response of the porous metal. The yield condition and the plastic flow rule are presented in the second part. The third part of the model is concerned with evolution laws for the internal variables. Finally, the elastic and plastic constitutive equations are combined in order to derive the rate form of the elastoplastic equations, which relate the rate of deformation $\bar{\mathbf{D}}$ to the Jaumman derivative $\overset{\triangledown}{\bar{\boldsymbol{\sigma}}}$ of the Cauchy (true) stress tensor $\bar{\boldsymbol{\sigma}}$.

2.1 Elastic constitutive relations

A hypoelastic form is assumed for the elastic part of the rate-of-deformation tensor:

$$\bar{\mathbf{D}}^e=\tilde{\mathbf{M}}\overset{\circ}{\bar{\boldsymbol{\sigma}}}, \tag{2}$$

where $\tilde{\mathbf{M}}$ is the effective elastic compliance tensor and $\overset{\circ}{\bar{\boldsymbol{\sigma}}}$ is a rate of the Cauchy stress which is corotational with the spin of the voids, i.e.,

$$\overset{\circ}{\bar{\boldsymbol{\sigma}}}=\dot{\bar{\boldsymbol{\sigma}}}-\boldsymbol{\omega}\bar{\boldsymbol{\sigma}}+\bar{\boldsymbol{\sigma}}\boldsymbol{\omega} \tag{3}$$

where $\boldsymbol{\omega}$ is the spin of the voids relative to a fixed laboratory frame. It is such that $\dot{\mathbf{n}}^{(i)}=\boldsymbol{\omega}\mathbf{n}^{(i)}$, where the three vectors $\mathbf{n}^{(i)}$ $(i=1,2,3)$ form an orthonormal basis, serving to define locally the principal axes of the ellipsoidal voids. The tensor $\boldsymbol{\omega}$, which corresponds to what is normally called the "microstructural spin", is calculated in subsection 2.3 on microstructure evolution (equation(16)).

Making use of the simplifying assumption discussed earlier about the shape and orientation of the void distribution, the effective compliance tensor may be written as

$$\tilde{\mathbf{M}} = \mathbf{M} + \frac{f}{1-f}\mathbf{Q}^{-1}. \tag{4}$$

In this expression, $\mathbf{M}$ is the elastic compliance tensor of the matrix material, which is the inverse of its elastic modulus tensor $\mathbf{L}$:

$$\mathbf{L} = 2\mu\mathbf{K} + 3\kappa\mathbf{J}, \qquad \mathbf{M} = \mathbf{L}^{-1} = \frac{1}{2\mu}\mathbf{K} + \frac{1}{3\kappa}\mathbf{J},$$
$$\mathbf{J} = \frac{1}{3}\boldsymbol{\delta}\otimes\boldsymbol{\delta}, \qquad \mathbf{K} = \mathbf{I} - \mathbf{J}, \tag{5}$$

where μ and κ denote the elastic shear and bulk moduli of the matrix, and $\boldsymbol{\delta}$ and $\mathbf{I}$, the second- and symmetric fourth-order identity tensors. Also, f is the porosity and $\mathbf{Q}$ is a microstructural tensor Willis (1977), which is related to the tensor $\mathbf{S}$ of Eshelby (1957) via the relation

$$\mathbf{Q} = \mathbf{L}(\mathbf{I} - \mathbf{S}). \tag{6}$$

An expression for $\mathbf{Q}$ is given in the Appendix; more explicit expressions for $\mathbf{S}$ may be found in the original reference Eshelby (1957). Note that $\mathbf{S}$, and therefore $\mathbf{Q}$, depend on the shape and orientation of the ellipsoidal voids. Thus, the relevant internal variables characterizing the state of the microstructure in the porous metal are indeed the porosity (f), the two aspect ratios (w_1 and w_2) of the ellipsoidal voids, and the orientation of the voids as defined by the vectors $\mathbf{n}^{(i)}$ ($i = 1,2,3$). Note that only three scalar quantities are required to completely specify these vectors; they could be written, for example, in terms of three Euler angles: θ, ϕ and ψ [see Kailasam and Ponte Castañeda (1998)]. For convenience, the following set of internal variables is defined:

$$\mathbf{s} = \left(f, w_1, w_2, \mathbf{n}^{(1)}, \mathbf{n}^{(2)}, \mathbf{n}^{(3)}\right). \tag{7}$$

It is important to emphasize that the components of $\tilde{\mathbf{M}}$ in expression (4) are not constants; they depend on the porosity, and the shape and orientation of the voids, which evolve in time. It is also recalled that the hypoelastic form (2) is consistent, to leading order, with hyperelastic behavior, because the elastic strains in porous metals are small relative to the plastic strains [see Needleman (1985); Aravas (1992)].

2.2 Yield condition and plastic flow rule

Next, expressions are given to characterize the plastic part of the macroscopic deformation for the porous metal. The constitutive behavior of the matrix phase could be taken to be of a fairly general type, including rate-dependent and hardening effects. However, as the main goal of this work is to investigate the effect of microstructure evolution, the matrix phase is taken to be isotropic and ideally plastic. Then, the nonlinear variational procedure of Ponte Castañeda (1991) allows the calculation of an effective yield function for the porous material in terms of the effective viscous compliance tensor of a fictitious linear comparison porous material which has the same microstructure as the perfectly plastic porous material. Thus, the effective yield function can be written in the form:

$$\tilde{\Phi}(\bar{\boldsymbol{\sigma}}, \mathbf{s}) = \frac{\bar{\boldsymbol{\sigma}}\cdot(\tilde{\mathbf{m}}(\mathbf{s})\bar{\boldsymbol{\sigma}})}{1-f} - (\sigma_y)^2, \tag{8}$$

where σ_y is the yield strength in tension of the matrix material. In the above expression, $\tilde{\mathbf{m}}$ corresponds to an appropriately normalized effective viscous compliance tensor $\tilde{\mathbf{m}}$ for the fictitious linear comparison porous material. It is given by

$$\tilde{\mathbf{m}}(\mathbf{s}) = 3\mu\tilde{\mathbf{M}}|_{\kappa\to\infty} = \frac{3}{2}\mathbf{K} + \frac{f}{1-f}3\mu\mathbf{Q}^{-1}|_{\kappa\to\infty}, \tag{9}$$

where the expression for $\tilde{\mathbf{M}}$ is precisely the same as in (4). However, because of the assumed plastic incompressibility of the matrix phase, the limit as $\kappa\to\infty$ must be taken in the expression (4) for $\tilde{\mathbf{M}}$. This limiting process, which is complicated by the fact that the hydrostatic component of $\mathbf{L}$ blows up in the definition (6) of the tensor $\mathbf{Q}$, can be evaluated more conveniently by considering the more explicit expressions for $\mathbf{Q}$ given in the Appendix. It follows that $\tilde{\Phi}$ is only a function of $\bar{\boldsymbol{\sigma}}$, the microstructural variables $\mathbf{s}$ and the yield strength of the matrix phase σ_y. In the most general case, $\tilde{\Phi}$ exhibits orthotropic symmetry with symmetry axes aligned with the axes of the voids, i.e., aligned with the vectors $\mathbf{n}^{(i)}$ ($i = 1,2,3$). It is emphasized that the plastic behavior described by the macroscopic potential $\tilde{\Phi}$ is fully *compressible*, in agreement with experimental observations Ponte Castañeda and Zaidman (1994).

At this point, it is emphasized that although the matrix material here has been taken to be elastic-perfectly plastic, it is possible to incorporate hardening effects in a straightforward manner by treating the yield strength σ_y of the matrix material as a function of a properly defined "equivalent plastic strain" $\bar{\varepsilon}^p$, as is done, for example by Hill (1950). In such a case, $\bar{\varepsilon}^p$ is an additional internal variable to the model.

The plastic rate-of-deformation tensor $\bar{\mathbf{D}}^p$ is obtained in terms of $\tilde{\Phi}$ from the relation

$$\bar{\mathbf{D}}^p = \dot{\Lambda}\mathbf{N}, \qquad \mathbf{N} = \frac{\partial\tilde{\Phi}}{\partial\bar{\boldsymbol{\sigma}}}, \tag{10}$$

where $\dot{\Lambda} \geq 0$ is the plastic multiplier, which depends on the matrix hardening and the evolution of the microstructure and is obtained from the "consistency condition" as discussed in subsection 2.4 .

2.3 Evolution of the microstructure

When the porous material deforms, the state variables evolve and, in turn, influence the response of the material. In the current application to porous metals, it is assumed that all the

changes in the microstructure occur only due to the plastic deformation of the material. This is expected to be reasonable, because the elastic strains here are relatively small compared to the plastic strains. The evolution equations for these variables can then be determined from the kinematics of the deformation by assuming that, on the average, the evolution of the relevant internal variables is characterized by the average deformation and spin fields in the void phase, and making use of the aforementioned homogenization procedure to estimate consistently the average rate of deformation and spin in the voids Ponte Castañeda and Zaidman (1994); Kailasam and Ponte Castañeda (1998).

In view of the plastic incompressibility of the matrix phase, the evolution equation for the porosity f follows easily from the continuity equation and is given by

$$\dot{f} = (1-f)\,\bar{D}^p_{kk} = \dot{\Lambda}\,(1-f)\,N_{kk} \equiv \dot{\Lambda}\,h(\bar{\boldsymbol{\sigma}},\mathbf{s}). \tag{11}$$

Evolution equations for the aspect ratios of the voids w_1 and w_2 are obtained from the definition of the average value of the rate of deformation in the voids, given by $\mathbf{D}^p = \mathbf{A}\bar{\mathbf{D}}^p$, where $\mathbf{A}$ is the relevant strain-rate concentration tensor. The resulting equations are

$$\begin{aligned}\dot{w}_1 &= w_1\left(D^{p\,\prime}_{33} - D^{p\,\prime}_{11}\right) = \dot{\Lambda}\,w_1\left(A'_{33ij} - A'_{11ij}\right)N'_{ij}\\ &\equiv \dot{\Lambda}\,h_1(\bar{\boldsymbol{\sigma}},\mathbf{s}),\end{aligned} \tag{12}$$

$$\begin{aligned}\dot{w}_2 &= w_2\left(D^{p\,\prime}_{33} - D^{p\,\prime}_{22}\right) = \dot{\Lambda}\,w_2\left(A'_{33ij} - A'_{22ij}\right)N'_{ij}\\ &\equiv \dot{\Lambda}\,h_2(\bar{\boldsymbol{\sigma}},\mathbf{s}).\end{aligned} \tag{13}$$

In these relations, and for the rest of this section, primed quantities indicate components in a coordinate frame that coincides instantaneously with the local orientation of the voids, as determined by the vectors $\mathbf{n}^{(i)}$ $(i=1,\ldots,3)$. For example, $\mathbf{N} = \sum_{i,j} N'_{ij}\mathbf{n}^{(i)}\otimes\mathbf{n}^{(j)}$, $\mathbf{A} = \sum_{i,j,k,l} A'_{ijkl}\mathbf{n}^{(i)}\otimes\mathbf{n}^{(j)}\otimes\mathbf{n}^{(k)}\otimes\mathbf{n}^{(l)}$, etc. The strain-rate concentration tensor for the void phase is given by

$$\mathbf{A}(\mathbf{s}) = \left[\mathbf{I} - (1-f)\,\mathbf{S}\right]^{-1}|_{\kappa\to\infty}. \tag{14}$$

Note that $\mathbf{A}$ becomes independent of material properties and depends only on the microstructural variables $\mathbf{s}$. Again, it is emphasized that the strain-rate concentration tensor $\mathbf{A}$ is consistent with overall compressibility for the plastic deformation of the porous metal.

Finally, the evolution of the average void orientation is obtained from the relations

$$\dot{\mathbf{n}}^{(i)} = \boldsymbol{\omega}\mathbf{n}^{(i)} \quad (i=1,2,3), \tag{15}$$

where $\boldsymbol{\omega}$ is the spin of the Eulerian axes of the average deformation of the voids determined by the well-known kinematical relation Ogden (1984)

$$\omega'_{kl} = W'_{kl} - \frac{w_k^2+w_l^2}{w_k^2-w_l^2}D^{p\,\prime}_{kl}, \quad k\neq l, \quad w_3 = 1, \quad w_k \neq w_l. \tag{16}$$

In this relation, $\mathbf{D}^p = \mathbf{A}\bar{\mathbf{D}}^p$ as before, $\mathbf{W}$ is the average spin inside the void phase, and primed quantities indicate again components in a coordinate frame that coincides instantaneously with the local principal axes of the ellipsoidal voids. Note that the average spin in the void phase $\mathbf{W}$ is different from the "macroscopic", or "continuum" spin $\bar{\mathbf{W}}$. In fact, the homogenization analysis of Kailasam and Ponte Castañeda (1998) established that

$$\mathbf{W} = \bar{\mathbf{W}} - \mathbf{C}\bar{\mathbf{D}}^p, \tag{17}$$

where the spin-concentration tensor is given by

$$\mathbf{C}(\mathbf{s}) = (1-f)\,\boldsymbol{\Pi}\left[(1-f)\mathbf{S}-\mathbf{I}\right]^{-1}|_{\kappa\to\infty}. \tag{18}$$

Here $\boldsymbol{\Pi}$ is the Eshelby tensor serving to determine the spin of an isolated void in an infinite matrix. Again, because of the plastic incompressibility of the matrix phase, the limit as $\kappa\to\infty$ is taken, and $\boldsymbol{\Pi}$ becomes independent of material properties. It follows that the spin-concentration tensor $\mathbf{C}$ depends only on the microstructural variables $\mathbf{s}$.

It should be noted that equation (15) can be written also in the form

$$\mathring{\mathbf{n}}^{(i)} = \mathbf{0}, \tag{19}$$

where $\mathring{\mathbf{n}}^{(i)}$ is the rate of $\mathbf{n}^{(i)}$ corotational with the spin of the voids, i.e.,

$$\mathring{\mathbf{n}}^{(i)} = \dot{\mathbf{n}}^{(i)} - \boldsymbol{\omega}\mathbf{n}^{(i)}. \tag{20}$$

The microstructural spin $\boldsymbol{\omega}$ can be used also to define the so-called "plastic spin" $\mathbf{W}^p$, which is the spin of the continuum relative to the microstructure Dafalias (1985), i.e.,

$$\mathbf{W}^p = \bar{\mathbf{W}} - \boldsymbol{\omega}. \tag{21}$$

Combination of the last equation with (17) and (16) leads to the expression

$$\mathbf{W}^p = \dot{\Lambda}\boldsymbol{\Omega}, \tag{22}$$

where $\boldsymbol{\Omega}$ is a second-order antisymmetric tensor with components

$$\begin{aligned}\Omega'_{kl} &= \left(C'_{klij} - \frac{w_k^2+w_l^2}{w_k^2-w_l^2}A'_{klij}\right)N'_{ij}, \quad k\neq l,\\ &w_k\neq w_l, \quad w_3 = 1 \quad (\text{no sum over } k,l).\end{aligned} \tag{23}$$

When two of the w_i are equal, say $w_1 = w_2$, the material becomes locally transversely isotropic about the $\mathbf{n}^{(3)}$-direction, and

$$\Omega^l_{kl} = 0, \qquad \text{when} \quad k \neq l, \quad w_k = w_l \quad (\text{with } w_3 = 1). \tag{24}$$

Finally, when all three aspect ratios are equal $(w_1 = w_2 = 1)$, the material is locally isotropic and Dafalias (1985)

$$\mathbf{W}^p = \mathbf{\Omega} = \mathbf{0}. \tag{25}$$

It should be noted that the constitutive functions $\tilde{\Phi}$, $\mathbf{N}$, h, h_1, h_2, and $\mathbf{\Omega}$ are isotropic functions of their arguments, i.e., they are such that

$$\tilde{\Phi}(\mathbf{R}\bar{\boldsymbol{\sigma}}\mathbf{R}^T, f, w_1, w_2, \mathbf{R}\,\mathbf{n}^{(i)}) = \tilde{\Phi}(\bar{\boldsymbol{\sigma}}, f, w_1, w_2, \mathbf{n}^{(i)}), \tag{26}$$

$$\mathbf{N}(\mathbf{R}\bar{\boldsymbol{\sigma}}\mathbf{R}^T, f, w_1, w_2, \mathbf{R}\,\mathbf{n}^{(i)}) = \mathbf{R}\mathbf{N}(\bar{\boldsymbol{\sigma}}, f, w_1, w_2, \mathbf{n}^{(i)})\,\mathbf{R}^T, \tag{27}$$

etc., for all orthogonal second-order tensors $\mathbf{R}$. The mathematical isotropy of the aforementioned functions guarantees the invariance of the constitutive equations under superposed rigid body rotations. It should be emphasized, however, that the material is *anisotropic*, due to the tensorial character of the $\mathbf{n}^{(i)}$'s.

Making use of relation (21) and of the Jaumann derivative of $\mathbf{n}^{(i)}$, given by $\overset{\triangledown}{\mathbf{n}}{}^{(i)} = \dot{\mathbf{n}}^{(i)} - \bar{\mathbf{W}}\mathbf{n}^{(i)}$, it is possible to write the evolution equation for the axes of anisotropy of the porous material in the form

$$\overset{\triangledown}{\mathbf{n}}{}^{(i)} = -\mathbf{W}^p\mathbf{n}^{(i)} = -\dot{\Lambda}\mathbf{\Omega}\mathbf{n}^{(i)}. \tag{28}$$

It follows that the evolution equations for all the microstructural variables $\mathbf{s}$, as given by relations (11), (12), (13), and (28) can be written compactly in the form

$$\overset{\triangledown}{\mathbf{s}} = \dot{\Lambda}\,\mathbf{g}\,(\bar{\boldsymbol{\sigma}}; \mathbf{s}), \tag{29}$$

where $\mathbf{g}$ is a collection of suitable isotropic functions. The plastic multiplier $\dot{\Lambda}$ can be computed from the so-called "consistency condition" as described in the following subsection.

In summary, constitutive laws have now been developed to describe the behavior of the elastic-plastic porous material. In the elastic regime the behavior is characterized by equations (2) to (6) and in the plastic regime by equations (8) to (10). The evolution of the microstructural variables $\mathbf{s}$, as defined by relation (7), is characterized by equations (11), (12), (13), and (28).

2.4 Rate form of the elastoplastic equations

The above-developed constitutive equations are now combined in order to derive an equation of the form

$$\overset{\triangledown}{\bar{\boldsymbol{\sigma}}} = \tilde{\mathbf{L}}^{ep}\bar{\mathbf{D}}, \tag{30}$$

where $\tilde{\mathbf{L}}^{ep}$ is the fourth-order tensor of the elastoplastic moduli of the porous metal. The derivation is as follows.

Substitution of $\bar{\mathbf{D}}^e = \bar{\mathbf{D}} - \bar{\mathbf{D}}^p = \bar{\mathbf{D}} - \dot{\Lambda}\mathbf{N}$ into (2) yields

$$\overset{\circ}{\bar{\boldsymbol{\sigma}}} = \tilde{\mathbf{L}}\bar{\mathbf{D}} - \dot{\Lambda}\tilde{\mathbf{L}}\mathbf{N}. \tag{31}$$

Since $\tilde{\Phi}$ is an isotropic function, the "consistency condition" $\dot{\tilde{\Phi}} = 0$ can be written in the form Dafalias (1985)

$$\dot{\tilde{\Phi}} = \frac{\partial\tilde{\Phi}}{\partial\bar{\boldsymbol{\sigma}}} \cdot \overset{\circ}{\bar{\boldsymbol{\sigma}}} + \frac{\partial\tilde{\Phi}}{\partial\mathbf{s}} \cdot \overset{\circ}{\mathbf{s}} = 0, \tag{32}$$

where $\overset{\circ}{\mathbf{s}} = (\dot{f}, \dot{w}_1, \dot{w}_2, \overset{\circ}{\mathbf{n}}{}^{(1)}, \overset{\circ}{\mathbf{n}}{}^{(2)}, \overset{\circ}{\mathbf{n}}{}^{(3)})$. In view of the fact that $\overset{\circ}{\mathbf{n}}{}^{(i)} = \mathbf{0}$ (eqn (19)), the last relation can be written as

$$\mathbf{N} \cdot \overset{\circ}{\bar{\boldsymbol{\sigma}}} + \frac{\partial\tilde{\Phi}}{\partial f}\dot{f} + \frac{\partial\tilde{\Phi}}{\partial w_1}\dot{w}_1 + \frac{\partial\tilde{\Phi}}{\partial w_2}\dot{w}_2 = 0. \tag{33}$$

Substitution of $\overset{\circ}{\bar{\boldsymbol{\sigma}}}$, $\dot{f}$, $\dot{w}_1$ and $\dot{w}_2$ from (31), (11), (12) and (13) into the last equation yields

$$\begin{aligned} &\mathbf{N} \cdot (\tilde{\mathbf{L}}\bar{\mathbf{D}}) - \dot{\Lambda}[\mathbf{N} \cdot (\tilde{\mathbf{L}}\mathbf{N}) + H_c] = 0, \\ &H_c = -\left(\frac{\partial\tilde{\Phi}}{\partial f}h + \frac{\partial\tilde{\Phi}}{\partial w_1}h_1 + \frac{\partial\tilde{\Phi}}{\partial w_2}h_2\right), \end{aligned} \tag{34}$$

from which it follows that

$$\begin{aligned} &\dot{\Lambda} = \frac{1}{L}\mathbf{N} \cdot (\tilde{\mathbf{L}}\bar{\mathbf{D}}) = \frac{1}{L}(\mathbf{N}\tilde{\mathbf{L}}) \cdot \bar{\mathbf{D}}, \\ &L = H_c + \mathbf{N} \cdot (\tilde{\mathbf{L}}\mathbf{N}). \end{aligned} \tag{35}$$

Substitution of $\dot{\Lambda}$ into (31) yields

$$\overset{\circ}{\bar{\boldsymbol{\sigma}}} = \left[\tilde{\mathbf{L}} - \frac{1}{L}(\tilde{\mathbf{L}}\mathbf{N}) \otimes (\mathbf{N}\tilde{\mathbf{L}})\right]\bar{\mathbf{D}}. \tag{36}$$

The Jaumann derivative $\overset{\triangledown}{\bar{\boldsymbol{\sigma}}}$ is related to $\overset{\circ}{\bar{\boldsymbol{\sigma}}}$ by the following expression

$$\begin{aligned} \overset{\triangledown}{\bar{\boldsymbol{\sigma}}} &= \overset{\circ}{\bar{\boldsymbol{\sigma}}} + \bar{\boldsymbol{\sigma}}\mathbf{W}^p - \mathbf{W}^p\bar{\boldsymbol{\sigma}} = \overset{\circ}{\bar{\boldsymbol{\sigma}}} + \dot{\Lambda}(\bar{\boldsymbol{\sigma}}\mathbf{\Omega} - \mathbf{\Omega}\bar{\boldsymbol{\sigma}}) \\ &= \overset{\circ}{\bar{\boldsymbol{\sigma}}} + \frac{1}{L}(\bar{\boldsymbol{\sigma}}\mathbf{\Omega} - \mathbf{\Omega}\bar{\boldsymbol{\sigma}})(\mathbf{N}\tilde{\mathbf{L}}) \cdot \bar{\mathbf{D}}. \end{aligned} \tag{37}$$

Finally, substitution of (36) into (37) yields the desired equation $\overset{\triangledown}{\bar{\boldsymbol{\sigma}}} = \tilde{\mathbf{L}}^{ep}\bar{\mathbf{D}}$ with

$$\tilde{\mathbf{L}}^{ep} = \tilde{\mathbf{L}} - \frac{1}{L}(\tilde{\mathbf{L}}\mathbf{N} - \bar{\boldsymbol{\sigma}}\mathbf{\Omega} + \mathbf{\Omega}\bar{\boldsymbol{\sigma}}) \otimes (\mathbf{N}\tilde{\mathbf{L}}). \tag{38}$$

3 Numerical Implementation of the Constitutive Model

In this section, the numerical integration of the constitutive equations is described. For simplicity, and since there is no chance of confusion between averages over the void phase and over the porous material, the overbars and tildes are dropped in

the presentation, so that, for example, the macroscopic strain rate $\bar{\mathbf{D}}$, stress $\bar{\boldsymbol{\sigma}}$ and yield function $\tilde{\Phi}$ are now written $\mathbf{D}$, $\boldsymbol{\sigma}$ and Φ, respectively. In a finite element environment, the solution is developed incrementally and the constitutive equations are integrated at the element Gauss integration points. Let $\mathbf{F}$ denote the deformation gradient tensor. At a given Gauss point, the solution $(\mathbf{F}_n, \boldsymbol{\sigma}_n, \mathbf{s}_n)$ at time t_n as well as the deformation gradient $\mathbf{F}_{n+1}$ at time t_{n+1} are known, and the problem is to determine $(\boldsymbol{\sigma}_{n+1}, \mathbf{s}_{n+1})$.

The time variation of the deformation gradient $\mathbf{F}$ during the time increment $[t_n, t_{n+1}]$ can be written as

$$\mathbf{F}(t) = \Delta\mathbf{F}(t)\mathbf{F}_n = \mathbf{R}(t)\mathbf{U}(t)\mathbf{F}_n, \qquad t_n \le t \le t_{n+1}, \tag{39}$$

where $\mathbf{R}(t)$ and $\mathbf{U}(t)$ are the rotation and right stretch tensors associated with $\Delta\mathbf{F}(t)$. The corresponding deformation rate $\mathbf{D}(t)$ and spin $\mathbf{W}(t)$ tensors are given by

$$\mathbf{D}(t) \equiv \left[\dot{\mathbf{F}}(t)\mathbf{F}^{-1}(t)\right]_s = \left[\Delta\dot{\mathbf{F}}(t)\Delta\mathbf{F}^{-1}(t)\right]_s, \tag{40}$$

and

$$\mathbf{W}(t) \equiv \left[\dot{\mathbf{F}}(t)\mathbf{F}^{-1}(t)\right]_a = \left[\Delta\dot{\mathbf{F}}(t)\Delta\mathbf{F}^{-1}(t)\right]_a, \tag{41}$$

where the subscripts s and a denote the symmetric and antisymmetric parts respectively of a tensor.

If it is assumed that the Lagrangian triad associated with $\Delta\mathbf{F}(t)$ (i.e., the eigenvectors of $\mathbf{U}(t)$) remains fixed in the time interval $[t_n, t_{n+1}]$, it can readily be shown that

$$\mathbf{D}(t) = \mathbf{R}(t)\dot{\mathbf{E}}(t)\mathbf{R}^T(t), \qquad \mathbf{W}(t) = \dot{\mathbf{R}}(t)\mathbf{R}^T(t), \tag{42}$$

and

$$\overset{\triangledown}{\boldsymbol{\sigma}}(t) = \mathbf{R}(t)\dot{\hat{\boldsymbol{\sigma}}}(t)\mathbf{R}^T(t), \qquad \overset{\triangledown}{\mathbf{n}}^{(i)}(t) = \mathbf{R}(t)\dot{\hat{\mathbf{n}}}^{(i)}(t), \tag{43}$$

where $\mathbf{E}(t) = \ln\mathbf{U}(t)$ is the logarithmic strain associated with the increment, $\hat{\boldsymbol{\sigma}}(t) = \mathbf{R}^T(t)\boldsymbol{\sigma}(t)\mathbf{R}(t)$, and $\hat{\mathbf{n}}^{(i)}(t) = \mathbf{R}^T(t)\mathbf{n}^{(i)}(t)$.

It is noted that at the start of the increment $(t = t_n)$

$$\mathbf{F}_n = \mathbf{R}_n = \mathbf{U}_n = \boldsymbol{\delta}, \qquad \hat{\boldsymbol{\sigma}}_n = \boldsymbol{\sigma}_n, \qquad \hat{\mathbf{n}}_n^{(i)} = \mathbf{n}_n^{(i)}, \quad \text{and} \quad \mathbf{E}_n = \mathbf{0}, \tag{44}$$

whereas at the end of the increment $(t = t_{n+1})$

$$\Delta\mathbf{F}_{n+1} = \mathbf{F}_{n+1}\mathbf{F}_n^{-1} = \mathbf{R}_{n+1}\mathbf{U}_{n+1} = \text{known}, \quad \text{and} \quad \mathbf{E}_{n+1} = \ln\mathbf{U}_{n+1} = \text{known}. \tag{45}$$

Taking into account that Φ, $\mathbf{N}$, h, h_1, h_2 and $\boldsymbol{\Omega}$ are isotropic functions of their arguments, the elastoplastic equations can be written in the form

$$\dot{\mathbf{E}} = \dot{\mathbf{E}}^e + \dot{\mathbf{E}}^p, \tag{46}$$

$$\dot{\hat{\boldsymbol{\sigma}}} = \hat{\mathbf{L}}\dot{\mathbf{E}}^e + \dot{\Lambda}\left[\hat{\boldsymbol{\sigma}}\boldsymbol{\Omega}(\hat{\boldsymbol{\sigma}}, \hat{\mathbf{s}}) - \boldsymbol{\Omega}(\hat{\boldsymbol{\sigma}}, \hat{\mathbf{s}})\hat{\boldsymbol{\sigma}}\right], \tag{47}$$

$$\Phi(\hat{\boldsymbol{\sigma}}, \hat{\mathbf{s}}) = 0, \tag{48}$$

$$\dot{\mathbf{E}}^p = \dot{\Lambda}\mathbf{N}(\hat{\boldsymbol{\sigma}}, \hat{\mathbf{s}}), \tag{49}$$

$$\dot{f} = \dot{\Lambda}h(\hat{\boldsymbol{\sigma}}, \hat{\mathbf{s}}), \tag{50}$$

$$\dot{w}_1 = \dot{\Lambda}h_1(\hat{\boldsymbol{\sigma}}, \hat{\mathbf{s}}), \tag{51}$$

$$\dot{w}_2 = \dot{\Lambda}h_2(\hat{\boldsymbol{\sigma}}, \hat{\mathbf{s}}), \tag{52}$$

$$\dot{\hat{\mathbf{n}}}^{(i)} = -\dot{\Lambda}\boldsymbol{\Omega}(\hat{\boldsymbol{\sigma}}, \hat{\mathbf{s}})\hat{\mathbf{n}}^{(i)}, \tag{53}$$

where $\hat{L}_{ijkl} = R_{mi}R_{nj}R_{pk}R_{ql}L_{mnpq}$ and $\hat{\mathbf{s}} = (f, w_1, w_2, \hat{\mathbf{n}}^{(1)}, \hat{\mathbf{n}}^{(2)}, \hat{\mathbf{n}}^{(3)})$.

Integration of equation (46) gives

$$\Delta\mathbf{E} = \Delta\mathbf{E}^e + \Delta\mathbf{E}^p, \qquad \text{or} \qquad \Delta\mathbf{E}^e = \Delta\mathbf{E} - \Delta\mathbf{E}^p, \tag{54}$$

where the notation $\Delta A = A_{n+1} - A_n$ is used. The forward Euler method is used for the numerical integration of equations (47) and (49):

$$\hat{\boldsymbol{\sigma}}_{n+1} = \boldsymbol{\sigma}_n + \mathbf{L}_n\Delta\mathbf{E}^e + \Delta\Lambda\left(\boldsymbol{\sigma}_n\boldsymbol{\Omega}_n - \boldsymbol{\Omega}_n\boldsymbol{\sigma}_n\right), \tag{55}$$

$$\Delta\mathbf{E}^p = \Delta\Lambda\mathbf{N}_n, \tag{56}$$

where use has been made of the fact that $\hat{\mathbf{L}}_n = \mathbf{L}_n$. Then, using (54) and (56), equation (55) can be written as

$$\hat{\boldsymbol{\sigma}}_{n+1}(\Delta\Lambda) = \boldsymbol{\sigma}_n + \mathbf{L}_n(\Delta\mathbf{E} - \Delta\Lambda\mathbf{N}_n) + \Delta\Lambda\left(\boldsymbol{\sigma}_n\boldsymbol{\Omega}_n - \boldsymbol{\Omega}_n\boldsymbol{\sigma}_n\right). \tag{57}$$

The evolution equations of the internal variables f, w_1 and w_2 are also integrated by using a forward Euler scheme:

$$f_{n+1}(\Delta\Lambda) = f_n + \Delta\Lambda h(\boldsymbol{\sigma}_n, \mathbf{s}_n), \tag{58}$$

$$(w_1)_{n+1}(\Delta\Lambda) = (w_1)_n + \Delta\Lambda h_1(\boldsymbol{\sigma}_n, \mathbf{s}_n), \tag{59}$$

$$(w_2)_{n+1}(\Delta\Lambda) = (w_2)_n + \Delta\Lambda h_2(\boldsymbol{\sigma}_n, \mathbf{s}_n), \tag{60}$$

Also, the evolution equation for $\hat{\mathbf{n}}^{(i)}$ is approximated by

$$\dot{\hat{\mathbf{n}}}^{(i)} = -\frac{\Delta\Lambda}{\Delta t}\boldsymbol{\Omega}_n\hat{\mathbf{n}}^{(i)}, \tag{61}$$

which, in turn, can be integrated exactly to give[4]

$$\hat{\mathbf{n}}_{n+1}(\Delta\Lambda) = \exp(-\Delta\Lambda\boldsymbol{\Omega}_n)\mathbf{n}_n^{(i)}. \tag{62}$$

The exponential of an antisymmetric second-order tensor $\mathbf{A}$ ($\mathbf{A}^T = -\mathbf{A}$) is an orthogonal tensor that can be determined

[4] Note that direct application of the forward Euler scheme in (53) would give $\hat{\mathbf{n}}_{n+1} = (\boldsymbol{\delta} - \Delta\Lambda\boldsymbol{\Omega}_n)\mathbf{n}_n$, where $\boldsymbol{\delta} - \Delta\Lambda\boldsymbol{\Omega}_n$ is a two-term approximation of the orthogonal tensor $\exp(-\Delta\Lambda\boldsymbol{\Omega}_n)$. Use of this approach would not keep the $\hat{\mathbf{n}}^{(i)}$'s unit vectors.

from the following formula, which is often attributed to Rodrigues,

$$\exp(\mathbf{A}) = \boldsymbol{\delta} + \frac{\sin a}{a}\mathbf{A} + \frac{1-\cos a}{a^2}\mathbf{A}^2, \tag{63}$$

where $a = \sqrt{A_{ij}A_{ij}/2}$ is the magnitude of the axial vector of $\mathbf{A}$.

Equations (57)–(60) and (62) define the quantities $\hat{\boldsymbol{\sigma}}_{n+1}$ and $\hat{\mathbf{s}}_{n+1}$ in terms of $\Delta\Lambda$. Finally, substitution of $\hat{\boldsymbol{\sigma}}_{n+1}(\Delta\Lambda)$ and $\hat{\mathbf{s}}_{n+1}(\Delta\Lambda)$ in the yield condition (48) gives an equation of the form

$$\Phi(\hat{\boldsymbol{\sigma}}_{n+1}(\Delta\Lambda), \hat{\mathbf{s}}_{n+1}(\Delta\Lambda)) = 0. \tag{64}$$

The above equation is an algebraic equation which is solved for $\Delta\Lambda$ by using the secant method. Once $\Delta\Lambda$ is found, equations (57)–(60) and (62) define $\hat{\boldsymbol{\sigma}}_{n+1}$, f_{n+1}, $(w_1)_{n+1}$, $(w_2)_{n+1}$, $\hat{\mathbf{n}}^{(1)}_{n+1}$, $\hat{\mathbf{n}}^{(2)}_{n+1}$, and $\hat{\mathbf{n}}^{(3)}_{n+1}$. Finally, $\boldsymbol{\sigma}_{n+1}$ and $\mathbf{n}^{(i)}_{n+1}$ are computed from

$$\boldsymbol{\sigma}_{n+1} = \mathbf{R}_{n+1}\hat{\boldsymbol{\sigma}}_{n+1}\mathbf{R}^T_{n+1}, \quad \text{and} \quad \mathbf{n}^{(i)}_{n+1} = \mathbf{R}_{n+1}\hat{\mathbf{n}}^{(i)}_{n+1}, \tag{65}$$

which completes the integration process.

4 Applications

The constitutive model presented in the previous sections is implemented in the ABAQUS general purpose finite element program Hibbitt (1984). This code provides a general interface so that a particular constitutive model can be introduced as a "user subroutine". The integration of the elastoplastic equations is carried out using the algorithm presented in section 3. The finite element formulation is based on the weak form of the momentum balance, the solution is carried out incrementally, and the discretized nonlinear equations are solved using Newton's method. In the calculations, the Jacobian of the Newton scheme is approximated by the tangent stiffness matrix derived using the moduli $\tilde{\mathbf{L}}^{ep}$ given by equation (38). Such an approximation of the Jacobian is first order accurate as $\Delta t \to 0$; it should be emphasized, however, that the aforementioned approximation influences only the rate of convergence of the Newton loop and not the accuracy of the results.

In the following examples, a porous material with initial porosity $f_0 = 0.15$ is used. The matrix material is elastic-perfectly plastic with yield stress in tension σ_y, Young's modulus $E = 300\,\sigma_y$, and Poisson's ratio $\nu = 0.49$. The porous material is assumed to be composed initially of a statistically isotropic distribution of spherical voids, i.e., the initial values of the aspect ratios w_1 and w_2 are $(w_1)_0 = (w_2)_0 = 1$.

In the finite element calculations, during the first increment of plastic deformation at a material point, the material is isotropic, and the $\mathbf{n}^{(i)}$'s are not defined. In such a case the calculations are carried out as follows. If $\Delta\mathbf{F}_1$ is the value of the deformation gradient associated with the first plastic increment at a material point, then the $\mathbf{n}^{(i)}$'s at the end of that increment are identified with the unit eigenvectors of the left-stretch-tensor $\mathbf{B} = \Delta\mathbf{F}_1\Delta\mathbf{F}_1^T$. For subsequent increments, the evolution of the $\mathbf{n}^{(i)}$'s is determined by using equations (62) and (65b).

4.1 Applications to a Plane Strain Extrusion Process

ABAQUS is used to analyze a plane strain extrusion process with a height reduction $\Delta h = 0.6\,h_0$, where h_0 is the initial height of the specimen (see Fig.1). The die is shaped linearly and the length of the reduction region is taken to be $L = 3h_0$. For more comprehensive results, including 20% and 40% reduction ratios, as well as axisymmetric extrusion processes, the reader is referred to Kailasam (1998). The driving force is provided by a rigid smooth piston acting against the rear face of the billet. The effects of friction along the metal-die interface are neglected.

The analysis is carried out with four-node isoparametric plane strain elements with 2×2 Gauss integration. In the finite element calculations all tensor components are calculated with respect to a fixed Cartesian coordinate system $Ox_1x_2x_3$ with base vectors $\mathbf{e}_1$, $\mathbf{e}_2$ and $\mathbf{e}_3$. The position $x_2 = 0$ defines the start of the reduction region. The material undergoes plane strain deformation on the $x_2 - x_3$ plane, and the unit vectors $\mathbf{n}^{(i)}$, that define the local orientation of the voids, can be written as

$$\mathbf{n}^{(1)} = \mathbf{e}_1, \tag{66}$$

$$\mathbf{n}^{(2)} = \cos\theta\,\mathbf{e}_2 + \sin\theta\,\mathbf{e}_3, \tag{67}$$

$$\mathbf{n}^{(3)} = -\sin\theta\,\mathbf{e}_2 + \cos\theta\,\mathbf{e}_3, \tag{68}$$

where θ is the angle between $\mathbf{n}^{(2)}$ and the direction of extrusion (axis Ox_2) and defines the orientation of the voids on the $x_2 - x_3$ plane.

With the objective of assessing the new features of the constitutive model proposed in this work, and in particular the implications of the evolution of the anisotropy, three models are used to characterize the response of the porous material:

(i) The general anisotropic constitutive theory developed in Section 2, which is referred to as the "anisotropic" model.

(ii) A special case of the general constitutive theory developed in Section 2, consisting in fixing the aspect ratios of the voids to remain spherical ($w_1 = w_2 = 1$), which is referred to as the "isotropic" model.

(iii) The Gurson (1977) theory for porous metals, which is referred to as the "Gurson" model.

Note that for the Gurson and isotropic models, there is only one state variable — the porosity, the shape of the voids being taken to be spherical throughout the deformation process.

The mesh at the end of the extrusion process is shown in Figure 1. Due to the symmetry of the problem, only the top half of

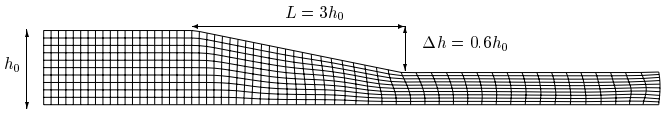

Figure 1 : The deformed finite element mesh.

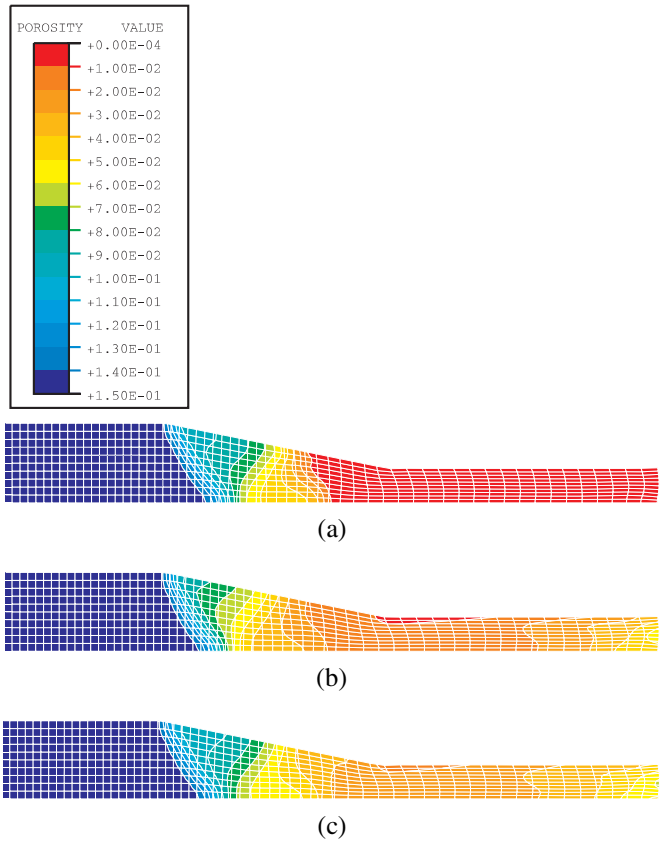

Figure 2 : Contour plots of porosity in the extruded specimen: (a) anisotropic constitutive theory, (b) Gurson theory, (c) isotropic theory.

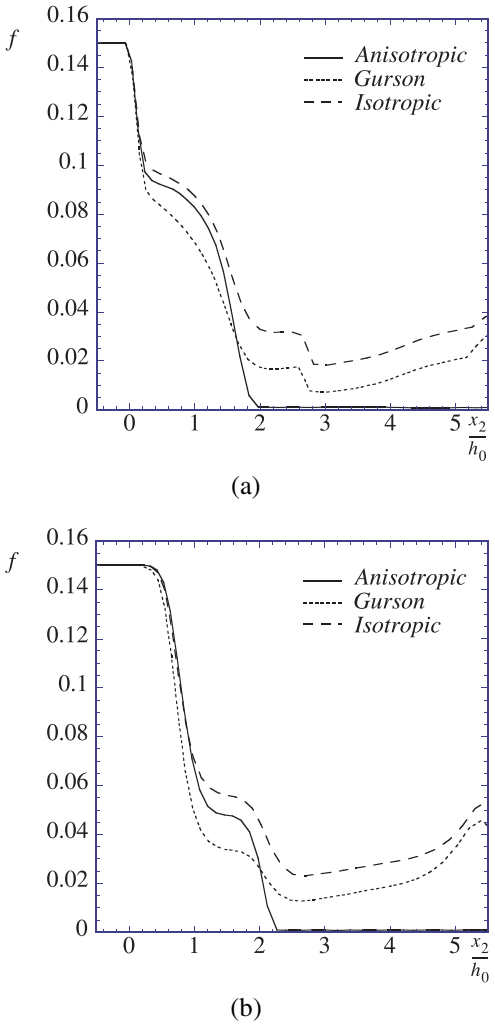

Figure 3 : Variation of porosity along the extrusion specimen: (a) variation along the top row of elements in Fig. 1, (b) variation along the bottom row of elements in Fig. 1.

the specimen is considered. The specimen is subjected to non-uniform loads during the extrusion process, and it is expected that the microstructure of the material evolves in a complex manner. For the anisotropic model, the decrease in porosity for this level of deformation is accompanied by the aspect ratios of the voids becoming very small (the voids tend to become cracks in certain parts of the specimen). As is known from earlier work, numerical difficulties can arise while modeling the microstructural changes in this limiting case. To avoid these difficulties, the porosity and the aspect ratio of the voids were not allowed to continue to change once the porosity reached a level of 0.1% ($f = 0.001$). However, the predictions that are generated by making use of this approximation are still expected to be quite accurate.

Figures 2 and 3 show comparisons of the porosity distributions predicted by the three models. Figure 2 shows contour plots of the porosity throughout the specimen and Figure 3 shows the variation of the porosity along the top and bottom row of elements (which corresponds to the middle of the actual specimen). The anisotropic model predicts a smaller porosity throughout the specimen than that predicted by the Gurson or the isotropic models. In fact, the anisotropic model predicts that the material becomes fully dense ($f \leq 0.001$) even before the specimen exits the die, while the other models predict a small, but finite, porosity at the end of the process (the Gurson model predicts a minimum porosity of 0.006, while the isotropic model predicts a minimum of 0.024). The average porosity predicted by the anisotropic model across a section of the material undergoing steady deformation is 0.001, while the Gurson and the isotropic models predict 0.012 and 0.022, respectively. These results are consistent with the predictions

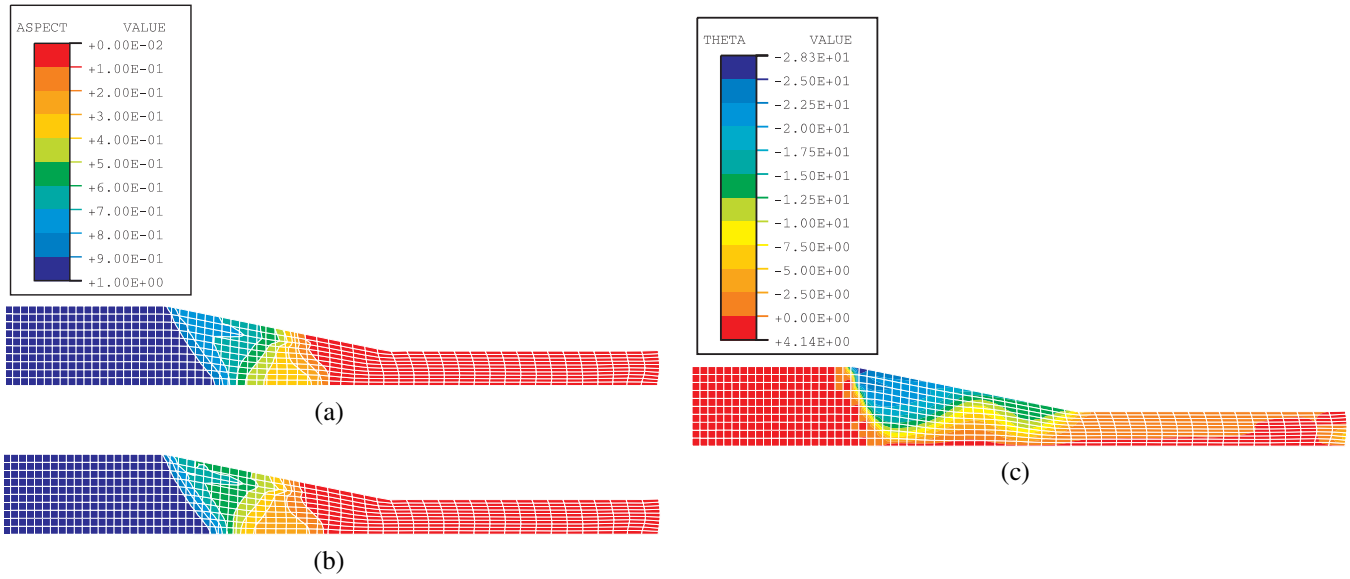

Figure 4 : Contour plots of the anisotropic state variables: (a) variation of the out-of-plane aspect ratio w_1, (b) variation of the in-plane aspect ratio w_2, (c) angle θ (in degrees) that defines the orientation of the voids relative to the direction of extrusion (axis Ox_2) on the plane of deformation.

of Ponte Castañeda and Zaidman (1994), who observed that, for uniform loading conditions, the change in shape of the voids could lead to much larger changes in porosity than when the voids are fixed to remain spherical, particularly in situations where the stress triaxialities are small. It is further noted that the isotropic version of the model of Kailasam and Ponte Castañeda (1998) is known to be stiffer than the Gurson model (which is also isotropic, as noted already), especially for hydrostatic loading conditions where the Gurson model is known to be very accurate. This would suggest that, in fact, the actual porosity reduction relative to the Gurson model may be larger than predicted by the anisotropic model. For the extrusion problem considered here, it was found that the stress triaxialities are small enough to make the effects of the changes in the shapes of the voids significant.

Figure 4 shows contour plots of the anisotropy variables in the specimen. It can be seen that the aspect ratios of the voids are indeed very small — the average value of the out-of-plane aspect ratio $w_1 = c/a$ across a transverse cross-section is 0.032 and that for the in-plane aspect ratio $w_2 = c/b$ is 0.018 (recall that the aspect ratios are not allowed to change for $f \leq 0.001$). The longest principal axis of the voids lies on the $x_2 - x_3$ plane and is aligned locally with $\mathbf{n}^{(2)}$. The orientation of the voids is determined by the angle θ, which becomes now the angle between the longest local principal axis of the voids and the extrusion direction (see eqn (67)). The orientation of the voids in the extrusion zone has a rather complex distribution — the voids are flattened and aligned with the extrusion direction at the middle of the specimen, and are oriented at different angles as we move towards the top of the specimen. It is also observed

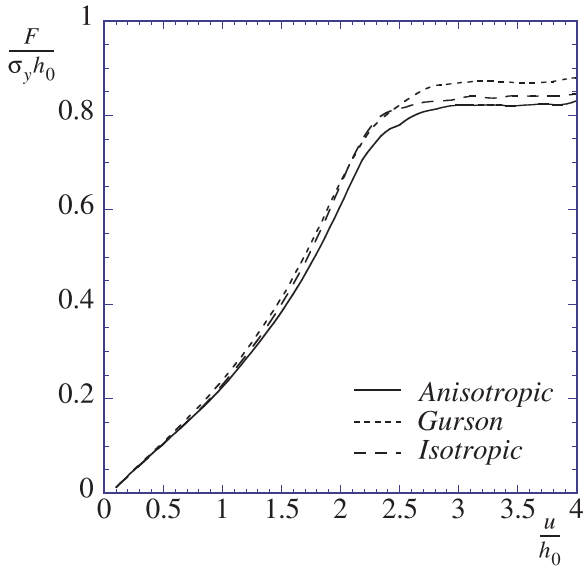

Figure 5 : The normalized extrusion force as a function of the normalized piston displacement.

that when the material exits the die, the voids are more or less flattened, and aligned with the extrusion direction.

Figure 5 shows the normalized extrusion force $F/(\sigma_y h_0)$ as a function of the normalized piston displacement u/h_0 for all three cases. It is observed that the force increases as the material deforms and reaches a steady value, when the deformation process also becomes steady. The force predicted by the anisotropic model is the least, while that predicted by the Gur-

son model is the largest—the steady force in the anisotropic case is about 6% less than that predicted by the Gurson model. This can be explained by recalling that the anisotropic model takes into account the changes in the shape and orientation of the voids, along with the changes in porosity. Although the decrease in the porosity tends to make the material response stiffer, the changes in shape and orientation of the voids tend to make the material more compliant, and, therefore, cause the extrusion force to be smaller for the anisotropic model than for the isotropic models.

It is noted that the isotropic model predicts a slightly smaller extrusion force than that predicted by the Gurson model, even though the Gurson model is known to predict a softer response than the isotropic model at high stress triaxialities Ponte Castañeda and Zaidman (1994). This can be explained by noting that the stress triaxialities in the present case are small enough so that the difference in the stiffness of the porous materials predicted by the two models (Gurson and isotropic) are not very different. Furthermore, it is observed that the average porosity in the specimen predicted by the isotropic model is larger than that predicted by the Gurson model (Figure 4), so that the effective response of the material tends to be softer (larger porosity implies softer material response). However, it is important to emphasize that the difference in the magnitude of the forces in the three cases is not very significant (less than 6%) for this level of deformation.

These observations are consistent with the predictions for the stresses across the specimen, shown in Figure 6, where it is shown that the stresses in the reduction region ($0 < x_2/h_0 < 3$) predicted by the anisotropic model are generally the least and those predicted by the Gurson model tend to be the largest.

The residual stresses in the specimen vary in a complex fashion for all three models; the residual tresses predicted by the anisotropic model tend to be larger that those predicted by the other two models, especially away from the center of the specimen. Figure 7 shows the predicted variation of the longitudinal stress $\bar{\sigma}_{22}$ across the section of the billet after the exit from the die ($x_2 = 4h_0$). These results are consistent with the earlier findings of Govindarajan (1992), who in addition to analyzing the extrusion of a Gurson type porous material using the finite element method, carried out an asymptotic analysis of the process Govindarajan and Aravas (1991). The quantitative differences between the predictions given here for the Gurson model and those arising from the implementation of Govindarajan (1992) are due to the differences in the initial porosities and die shapes.

4.2 Applications to Compaction of a Tapered Disk

In this section, the anisotropic constitutive theory is used to model the compaction of an axisymmetric tapered disk. Following Parteder (1998), the height of the disk is taken to be 80 mm, the diameters at the top and middle of the specimens, 60 and 120 mm, respectively, and the taper angle, 33.6 degrees.

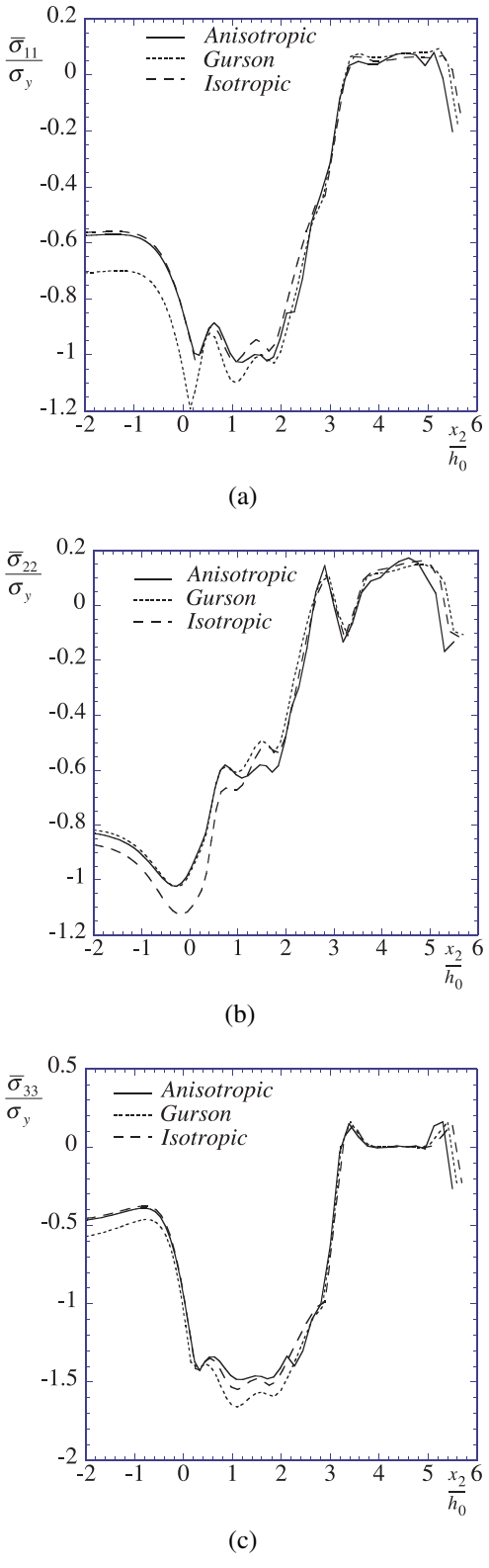

Figure 6 : Variation of the $\bar{\sigma}_{11}$, $\bar{\sigma}_{22}$, and $\bar{\sigma}_{33}$ stress components along the bottom row of elements of Fig. 1.

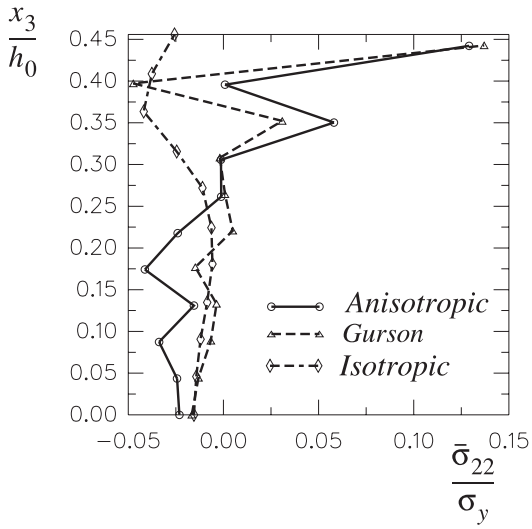

Figure 7 : Residual stress distribution across the section of the billet.

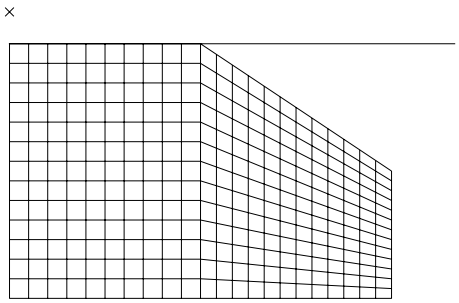

Figure 8 : The finite element mesh representing one quarter of a longitudinal section of the tapered disk.

The top surface of the disk is taken to be in contact with a rigid piston which is gradually moved downwards to simulate the compaction process. The coefficient of friction between the rigid piston and the disk is taken to be 0.08. Results are presented for the case where the height of the disk is reduced by 37.5 %. The predictions of the anisotropic constitutive theory are compared with results obtained by using the Gurson model and also with the experimental results of Zavaliangos and Anand (1993) (see also Haghi (1992), Parteder (1998) and Parteder et al. (1999)).

The analysis is carried out with four-node isoparametric axisymmetric elements with 2×2 Gauss integration. In the finite element calculations all tensor components are calculated with respect to a fixed Cartesian coordinate system Orx_2z with base vectors $\mathbf{e}_r$, $\mathbf{e}_2$ and $\mathbf{e}_z$. The axis Oz coincides with the axis of symmetry of the specimen, and the location $z = 0$ defines the plane of symmetry of the specimen that is normal to the axis

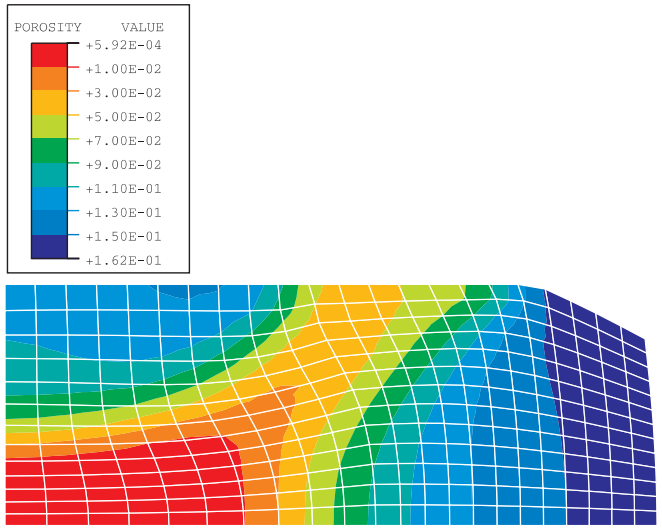

(a)

(b)

Figure 9 : Contour plots of porosity in the disk at a height reduction of 37.5%: (a) anisotropic model, (b) Gurson model.

of symmetry. The unit vectors $\mathbf{n}^{(i)}$, that define the local orientation of the voids, can be written as

$$\mathbf{n}^{(1)} = \cos\theta\,\mathbf{e}_r + \sin\theta\,\mathbf{e}_z, \tag{69}$$

$$\mathbf{n}^{(2)} = \mathbf{e}_2, \tag{70}$$

$$\mathbf{n}^{(3)} = -\sin\theta\,\mathbf{e}_r + \cos\theta\,\mathbf{e}_z, \tag{71}$$

where θ is the angle between $\mathbf{n}^{(1)}$ and the plane of symmetry $z = 0$, and defines the orientation of the voids on the longitudinal cross section of the disk. Due to symmetry considerations, only one quarter of the longitudinal cross-section of the disk is considered (see Figure 8).

Figures 9(a) and (b) show contour plots of porosity on a longitudinal cross-section of the disk, as predicted by the anisotropic and Gurson models. For the anisotropic model (part a), it is observed that regions close to the center of the disk are almost completely densified, whereas regions near the outer edges show an increase in porosity to a value of 16.2% (a value that is higher than the initial porosity of 15%). This variation of porosity in the specimen is caused by the nonuniform stresses and strains that develop inside the disk. In par-

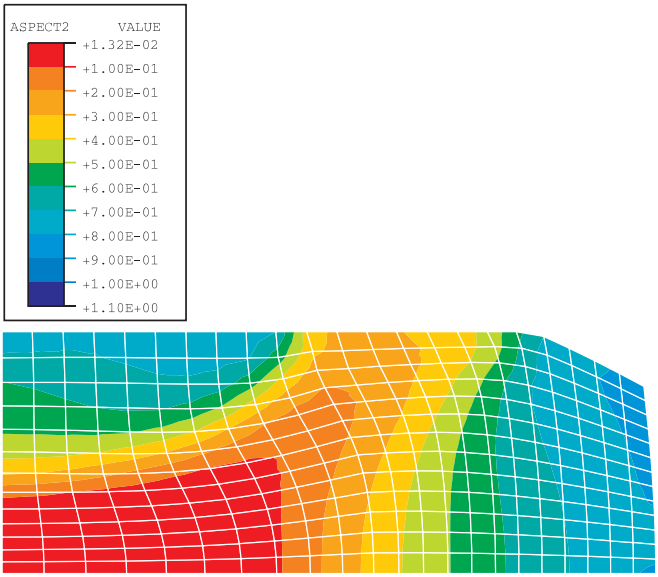

(a)

(b)

Figure 10 : Contour plots for the aspect ratios in the disk as predicted by the anisotropic model: (a) the in-plane aspect ratio, (b) the out-of-plane aspect ratio.

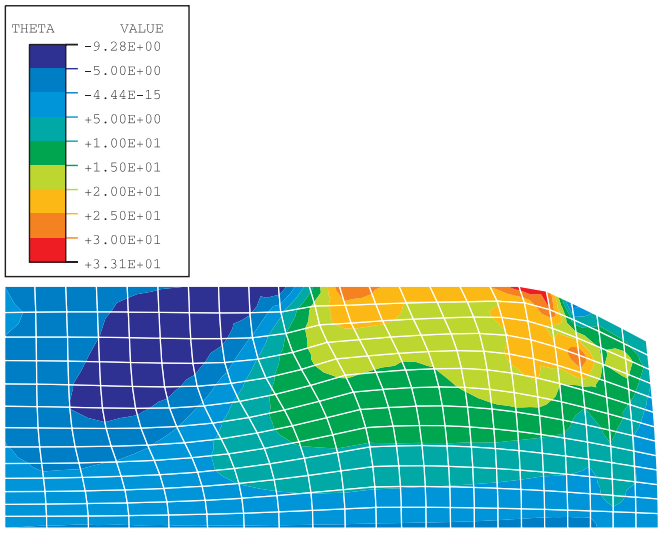

Figure 11 : Contour plots of the orientation of the voids as predicted by the anisotropic model. The angle θ (plotted in degrees) is the angle between the longest local principal direction of the voids and the horizontal direction.

ticular, as noted by Zavaliangos and Anand (1993), the hydrostatic component of the stress ranges from a highly compressive value near the center of the specimen to a slightly tensile value toward the outer edges. For the Gurson model, the predictions for the distribution of the porosity are qualitatively similar, but the predicted densification levels are significantly lower. For example, the anisotropic theory predicts that approximately 13% of the cross-sectional area of the disk near the center of the disk reaches a porosity level below 1%, whereas for the Gurson model the porosity in the same region attains values below only 5%, not reaching values below 1% anywhere in the disk. The greater amount of densification towards the center predicted by the anisotropic model is consistent with the experimental results of Zavaliangos and Anand (1993) and Parteder (1998). On the other hand, toward the outer edges of the specimen, the Gurson model generally predicts larger values of the porosity. This last observation is also in agreement with the results of Ponte Castañeda and Zaidman (1994), who observed that fixing the voids to remain spherical, as is the case with the Gurson model, results in an overestimation of the porosity for tensile loading conditions.

Figures 10(a) and (b) show contour plots of the pore in-plane $(w_1 = c/a)$ and out-of-plane $(w_2 = c/b)$ aspect ratios, respectively, as predicted by the anisotropic model. It is observed that the voids become increasingly flattened toward the center of the specimen, the aspect ratios reaching values of less than 0.1 for a region of about the same size as the region where the porosity reaches levels of less than 1%. On the other hand, the voids become slightly elongated toward the outer edges of the specimen. These predictions are consistent with the experimental observations of Zavaliangos and Anand (1993), and, to the best of our knowledge, this is the first time any theory has been able to predict this experimental fact. (Of course, the Gurson theory assumes *a priori* that the voids remain spherical throughout.) Figure 11 shows contour plots of θ, which is the angle between the longest local principal axis of the voids and the horizontal direction. It is noticed that the voids are aligned with the axes of the disk throughout most of the specimen. It is only towards the outer edges that the voids become tilted making angles of about 30° with respect to the horizontal.

Figure 12 shows the loads required for the compaction of the disk, as predicted by the anisotropic and the Gurson models. The response predicted by the anisotropic model tends to be softer than that predicted by the Gurson model. This is due to the higher degree of kinematic freedom of the anisotropic model which is better able to account for changes in the shape and orientation of the voids to accommodate the imposed deformation.

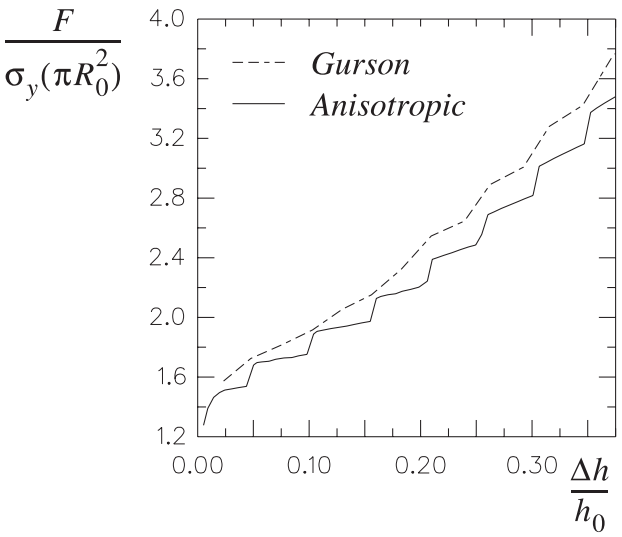

Figure 12 : Load-stroke curves as predicted by the anisotropic and Gurson models.

Acknowledgement: The work of MK and PPC was supported by AFOSR grant F49620-97-1-0212, NSF grant CMS-96-22714 and by ALCOA. We are grateful to Dr. E. Parteder (Technology Center, Pansee AG, Reutte, Austria) for supplying the ABAQUS input deck for the compaction simulation of the tapered disk and for valuable e-mail discussions.

References

Aravas, N. (1987): On the numerical integration of a class of pressure-dependent plasticity. *Int. J. Num. Meth. Engng.* **24**, 1395–1416.

Aravas, N. (1992): Finite elastoplastic transformations of transversely isotropic metals. *Int. J. Solids Structures* **29**, 2137–2157.

Dafalias, Y. F. (1985): The plastic spin. *J. Appl. Mech.* **52**, 865–871.

Eshelby, J. D. (1957): The determination of the elastic field of an ellipsoidal inclusion and related problems. *Proc. R. Soc. Lond. A* **241**, 376–396.

Govindarajan, R. M. and Aravas, N. (1991): Asymptotic analysis of extrusion of porous metals. *Int. J. Mech. Sci.* **33**, 505–527.

Govindarajan, S. (1992): *Deformation processing of porous metals*. Ph.D. thesis, University of Pennsylvania.

Gurson, A. L. (1977): Continuum theory of ductile rupture by void nucleation and growth: part I — Yield criteria and flow rules for porous ductile media. *J. Engng. Mater. Tech* **99**, 2–15.

Haghi, M. (1992): *Elasto-viscoplasticity of porous metals at elevated temperatures*. Ph.D. thesis, Massachusetts Institute of Technology.

Hibbitt, H. D. (1977): ABAQUS/EPGEN — A general purpose finite element code with emphasis in nonlinear applications. *Nucl. Engng. Des.* **7**, 271–297.

Hill, R. (1950): *The Mathematical Theory of Plasticity*. Oxford University Press, Oxford.

Hill, R. (1967): On the classical constitutive relations for elastic/plastic solids. *Recent Progress in Applied Mechanics: The Folke Odqvist Volume* (eds. B. Broberg, J. Hult and F. Niordson), 241–249, Almqvist and Wiksell/ Gebers Forlag, Stockholm, Sweden.

Kailasam, M. (1998): *A general constitutive theory for particulate composites and porous materials with evolving microstructures*. Ph.D. thesis, University of Pennsylvania.

Kailasam, M. and Ponte Castañeda, P. (1997): The evolution of anisotropy in porous materials and its implications for shear localization. *Mechanics of Granular and Porous Materials (IUTAM Symposium)* (eds. N. A. Fleck and A.C.F. Cocks), 365–376, Kluwer, Dordrecht, The Netherlands.

Kailasam, M. and Ponte Castañeda, P. (1998): A general constitutive theory for linear and nonlinear particulate media with microstructure evolution. *J. Mech. Phys. Solids.* **46**, 427–465.

Kailasam, M., Ponte Castañeda, P. and Willis, J. R. (1997a): The effect of particle size, shape, distribution and their evolution on the constitutive response of nonlinearly viscous composites – I. Theory. *Phil. Trans. R. Soc. Lond. A.* **355**, 1835–1852.

Kailasam, M., Ponte Castañeda, P. and Willis, J. R. (1997b): The effect of particle size, shape, distribution and their evolution on the constitutive response of nonlinearly viscous composites – II. Examples. *Phil. Trans. R. Soc. Lond. A.* **355**, 1853–1872.

Needleman, A. (1985): On finite element formulations for large elastic-plastic deformations. *Comput. Struct.* **20**.

Ogden, R. W. (1984): *Non-linear elastic deformations*. Ellis Horwood Series in Mathematics and its Applications., Halsted Press, New York.

Parteder, E. (1998): Private communication.

Parteder, E., Riedel, H. and Kopp, R. (1999): Densification of sintered molybdenum during hot upsetting experiments and modelling. *Mat. Sci. and Engrg.* **A264**, 17–25.

Ponte Castañeda, P. (1991): The effective mechanical properties of nonlinear isotropic solids. *J. Mech. Phys. Solids* **39**, 45–71.

Ponte Castañeda, P. and Willis, J. R. (1995): The effect of spatial distribution on the effective behavior of composite materials and cracked media. *J. Mech. Phys. Solids* **43**, 1919–1951.

Ponte Castañeda, P. and Zaidman, M. (1994): Constitutive models for porous materials with evolving microstructure. *J. Mech. Phys. Solids* **42**, 1459–1497.

Ponte Castañeda, P. and Zaidman, M. (1996): On the finite deformation of nonlinear composite materials. Part I- Instantaneous constitutive relations. *Int. J. Solids Structures* **33**, 1271–1286.

Suquet, P. (1985): Elements of homogenization for inelastic solid mechanics. *Homogenization techniques for Composite Media* (eds. E. Sanchez-Palencia and A. Zaoui), volume 272 of *Lecture Notes in Physics*, 194–280, Springer-Verlag, Germany.

Willis, J. R. (1977): Bounds and self-consistent estimates for the overall moduli of anisotropic composites. *J. Mech. Phys. Solids* **25**, 185–202.

Willis, J. R. (1978): Variational principles and bounds for the overall properties of composites. *Continuum Models for Discrete Systems* (ed. J. W. Prowan), 185–215, University of Waterloo Press.

Willis, J. R. (1981): Variational and related methods for the overall properties of composites. *Advances in Applied Mechanics* (ed. C.-S. Yih) Vol. 21, 2–74, Academic Press, Inc., London.

Zavaliangos, A. and Anand, L. (1993): Thermo-elasto-viscoplasticity of isotropic porous metals. *J. Mech. Phys. Solids* **41**, 185–202.

Appendix A: The Tensor Q

The tensor $\mathbf{Q}$ is most easily computed from the expression

$$\mathbf{Q} = \mathbf{L} - \mathbf{LPL} \tag{72}$$

in terms of the tensor $\mathbf{P} = \mathbf{SM}$, which is given in Willis (1977). The tensor $\mathbf{P}$ can be written in the form (e.g., see Willis, 1981)

$$\mathbf{P} = \frac{1}{4\pi|\mathbf{Z}|} \int\limits_{|\boldsymbol{\xi}|=1} \mathbf{H}(\boldsymbol{\xi})\, |\mathbf{Z}^{-1}\boldsymbol{\xi}|^{-3} dS(\boldsymbol{\xi}), \tag{73}$$

where

$$H_{ijkl}(\boldsymbol{\xi}) = \left[\mathbf{L}_2^{-1}(\boldsymbol{\xi})\right]_{ik} \xi_j \xi_l |_{(ij)(kl)}, \tag{74}$$

$$[\mathbf{L}_2(\boldsymbol{\xi})]_{ik} = L_{ijkl}\xi_j\xi_l, \tag{75}$$

$$\mathbf{Z} = w_1 \mathbf{n}^{(1)} \otimes \mathbf{n}^{(1)} + w_2 \mathbf{n}^{(2)} \otimes \mathbf{n}^{(2)} + \mathbf{n}^{(3)} \otimes \mathbf{n}^{(3)}, \tag{76}$$

and the notation

$$A_{(ij)(kl)} = \frac{1}{4}(A_{ijkl} + A_{ijlk} + A_{jikl} + A_{jilk}) \tag{77}$$

is used.

Since

$$\frac{1}{4\pi|\mathbf{Z}|} \int\limits_{|\boldsymbol{\xi}|=1} |\mathbf{Z}^{-1}\boldsymbol{\xi}|^{-3}\, dS(\boldsymbol{\xi}) = 1, \tag{78}$$

combination of (72) and (73) leads to following alternative expression for $\mathbf{Q}$

$$\mathbf{Q} = \frac{1}{4\pi|\mathbf{Z}|} \int\limits_{|\boldsymbol{\xi}|=1} \mathbf{E}(\boldsymbol{\xi})\, |\mathbf{Z}^{-1}\boldsymbol{\xi}|^{-3} dS(\boldsymbol{\xi}), \tag{79}$$

where

$$\mathbf{E}(\boldsymbol{\xi}) = \mathbf{L} - \mathbf{LH}(\boldsymbol{\xi})\mathbf{L}. \tag{80}$$

For isotropic materials $\mathbf{L} = 2\mu\mathbf{K} + 3\kappa\mathbf{J} = 2\mu\mathbf{I} + (\kappa - \frac{2}{3}\mu)\,\boldsymbol{\delta}\otimes\boldsymbol{\delta}$, so that

$$\mathbf{L}_2(\boldsymbol{\xi}) = \mu|\boldsymbol{\xi}|^2\boldsymbol{\delta} + \left(\kappa + \frac{1}{3}\mu\right)\boldsymbol{\xi}\otimes\boldsymbol{\xi}, \tag{81}$$

and

$$\mathbf{L}_2^{-1}(\boldsymbol{\xi}) = \frac{1}{\mu|\boldsymbol{\xi}|^4}\left[|\boldsymbol{\xi}|^2\boldsymbol{\delta} - \left(\frac{\kappa + \frac{1}{3}\mu}{\kappa + \frac{4}{3}\mu}\right)\boldsymbol{\xi}\otimes\boldsymbol{\xi}\right]. \tag{82}$$

Use of the last formula for $\mathbf{L}_2^{-1}(\boldsymbol{\xi})$ in (80) leads to following expression for the components of $\mathbf{E}(\boldsymbol{\xi})$

$$\begin{aligned} E_{pqrs}(\boldsymbol{\xi}) = \mu\{ & \delta_{pr}\delta_{qs} + \delta_{ps}\delta_{qr} \\ & - \frac{1}{|\boldsymbol{\xi}|^2}(\delta_{pr}\xi_q\xi_s + \delta_{ps}\xi_q\xi_r + \delta_{qr}\xi_p\xi_s + \delta_{qs}\xi_p\xi_r) \\ & + 2\left(\frac{\kappa - \frac{2}{3}\mu}{\kappa + \frac{4}{3}\mu}\right)\left[\delta_{pq}\delta_{rs} - \frac{1}{|\boldsymbol{\xi}|^2}(\delta_{pq}\xi_r\xi_s + \delta_{rs}\xi_p\xi_q)\right] \\ & + \frac{4}{|\boldsymbol{\xi}|^4}\left(\frac{\kappa + \frac{1}{3}\mu}{\kappa + \frac{4}{3}\mu}\right)\xi_p\xi_q\xi_r\xi_s\Big\}. \end{aligned}$$

Note that $\mathbf{Q}$ has the diagonal symmetry of an elasticity tensor. It is therefore easier to use than the Eshelby tensor $\mathbf{S}$ (Eshelby, 1957), to which it can be related via the expression $\mathbf{Q} = \mathbf{L}(\mathbf{I} - \mathbf{S})$. Note also that the incompressible limit (as $\kappa \to \infty$) can be generated easily from these expressions by replacing the terms in parentheses depending on κ by unity. The tensor $\mathbf{Q}$ may be given explicitly for the special cases of spherical and spheroidal inclusions. More generally, the double (surface) integral in expression (79) can be simplified to a single integral, the final result being expressible in terms of elliptic integrals, as is the case for the tensor $\mathbf{S}$ (Eshelby, 1957).